RSC Advances

PAPER

View Article Online
View Journal | View Issue

Cite this: *RSC Adv.*, 2020, **10**, 33033

Tunable surface wettability and pH-responsive 2D structures from amphiphilic and amphoteric protein microfibrils†

Xingchen Liu and You-Lo Hsieh *

Received 8th June 2020
Accepted 31st July 2020

DOI: 10.1039/d0ra05067a

rsc.li/rsc-advances

Two dimensional films and paper-like structures (60–170 μm thick) have been facilely fabricated by casting ethanolic dispersions of amphiphilic and amphoteric protein microfibrils (*ca.* 1.3 μm width; 53 μm length) under controlled temperatures and moisture levels. Surface hydrophilicity or hydrophobicity can be easily tuned by the abillity of the highly responsive microfibers to self-organize at the interface to mimic the hydrophilicity or hydrophobicity of cast substrates. For instance, surfaces cast on hydrophobic polystyrene or Teflon were moderately hydrophobic with water contact angles (WCAs) of 54°–71° while those on hydrophilic glass or exposed to air were hydrophilic (WCAs: 5°–10°). Thin film dried in the presence of moisture (60% RH) at 65 °C had the highest crystallinity (CrI: 56%) and β structure (64%), including 48% β-sheet form, and exhibited moisture-responsive T_g, pH-responsive planar swelling, and excellent wet resiliency in extremely acidic (pH = 0) to basic (pH = 10) conditions. The pH-dependent release of highly water-soluble cationic methylene blue bound to protein microfibril (SPMF) films attests to their amphoterism and demonstrates the applicability of such 2D structures for pH-dependent controlled release of other cationic and anionic species. Such versatility of amphiphilic and amphoteric protein microfibrils can be engineered into 2D structures with tunable surface hydrophilicity and hydrophobicity, moisture- and pH-responsive behaviors and controlled release capabilities.

Introduction

Polyelectrolytes exhibit pH-responsive behaviors due to the presence of either acidic (*i.e.* carboxyl, sulfonic, phosphate) or basic (pyridine, amine) functional groups that accept or donate protons in response to pH change.[1] Physiological environments of organs, tissues and cellular compartments are known to have different pHs, such as the highly acidic (pH = 2) stomach to the increasing basicity intestine (pH = 5–8),[2] making pH-responsive polymeric materials of interest for applications within the setting of biological conditions. Among biopolymers, some are anionic (*i.e.* alginate) or cationic (*i.e.* chitosan) polyelectrolytes but typically responsive in a specific and narrow range of pH around their pK_a.[2] Widening the pH responsiveness of biopolymers has been possible by crosslinking cationic chitosan with anionic carboxymethylcellulose[3] or carboxymethyl chitosan[4] and glutaraldehyde or guanidine hydrochloride (6 M) denatured soy proteins with epichlorohydrin.[5] However, the necessary chemical derivatives and acutely toxic chemical crosslinkers may limit their biological applications due to toxicity and biocompatibility concerns.

Soy proteins (SPs) contain amino acids with 18.0 mol% –NH_2 and 20.5 mol% –COOH and are the most abundant[6] and sustainable[7] natural polyampholytes. However, processing large, complex globular proteins such as SPs into any structure is challenging. We had previously validated a simple shear force process to disperse the complex and heterogeneous SPs into homogeneous aqueous colloids that exhibit the same amphiphilicity and amphoterism expected of the original SPs. With a 4.51 isoelectric point,[8] aq. SP colloids have been electrospun into ultra-fine (231 nm wide) fibers to exhibit excellent amphoteric characteristics to rapidly and selectively adsorb/desorb both cationic and anionic dyes.[9] As β-sheet secondary protein structures represent the most stable form as shown in spider silk proteins,[10] increasing such β structures may help to improve properties such as solubility and mechanically strength. Indeed, amphiphilic SP microfibrils (SPMFs) were robustly generated by ice-templating colloidal SPs to self-assembled laminated fibrous products and then selectively disassembling in polar liquids.[11] All these processes have involved only shear force and are completely aqueous. Further transforming the secondary structural transition of SPs into more β-sheets has the potential to render the whole matrix water-insoluble without needing additional chemical crosslinkers.

In this work, ethanol (EtOH) dispersion of 1.3 μm (±0.3 μm, N = 150) wide and 53 μm (±30 μm, N = 50) long SPMFs were

Department of Biological and Agricultural Engineering, University of California, Davis, California, 95616, USA. E-mail: ylhsieh@ucdavis.edu

† Electronic supplementary information (ESI) available. See DOI: 10.1039/d0ra05067a

cast into 2D thin sheets to investigate how hydrophobic or hydrophilic substrates and drying temperatures and moisture levels might influence their amphiphilic and amphoteric characteristics, secondary structure, and aqueous solubility. Surface morphology and wettability, moisture regain, and pH-responsive swelling behaviors of these 2D protein structures were thoroughly studied. The highly water-soluble cationic methylene blue (MB) was used as a model for the controlled release study *in vitro*. MB at 0.8 mM previously shown to be facilely bound to SPMFs by directly and homogeneously dispersing in colloids at 94.1% efficiency[10] was cast into 2D thin films. MB is a bio-active ingredient in pharmaceutical preparations,[12] a promising photosensitizer for catalysis, photodynamic therapy and wound healing, possessing a high quantum yield of $^1O_2$ generation with the excitation in the therapeutic window (600–900 nm). Immobilization of MB on a solid matrix is particularly of interest to avoid being reduced into the inactive leucomethylene blue in systemic administration.[11]

Results and discussions

Morphology and surface characteristics as affected by drying conditions and substrates

Ethanolic SPMF (1 w/v%) dispersions were cast in hydrophobic PS weight boats under ambient (21 °C) or elevated 65 °C temperatures, different moisture levels, and with or without vacuum to solidify (Table 1). At 21 °C, drying under vacuum shortened the time from 72 h (#1) to 16 h (#2) at 30% RH while higher moisture level of 75% RH lengthened the time to 48 h (#3). Elevating temperature to 65 °C lowered the moisture level to shorten drying time to 2 h (#4) while could also dry under vacuum even with added moisture (#5). All cast samples appeared relatively uniform macroscopically (Fig. 1). Faster drying under higher temperature and lower moisture level (#4) or at 21 °C under vacuum (#2), led to thicker (0.17 mm), opaque, and paper-like appearance whereas slowest ambient drying (#1) as well as both vacuum-and-moisture assisted drying (#3, #5), irrespective length of time, produced much thinner (0.06–0.09 mm) and translucent films, suggesting distinctively different association of individual SPMFs between these two groups. Slower drying (#1) or presence of moisture, either accelerated with vacuum (#3, #5) or elevated temperature (#5), allows reorganization and/or hydration of SPMFs to associate closely. Closer examination by SEM revealed smooth surfaces of the thinner translucent films (#1, #3, #5) in contrast to the rough,

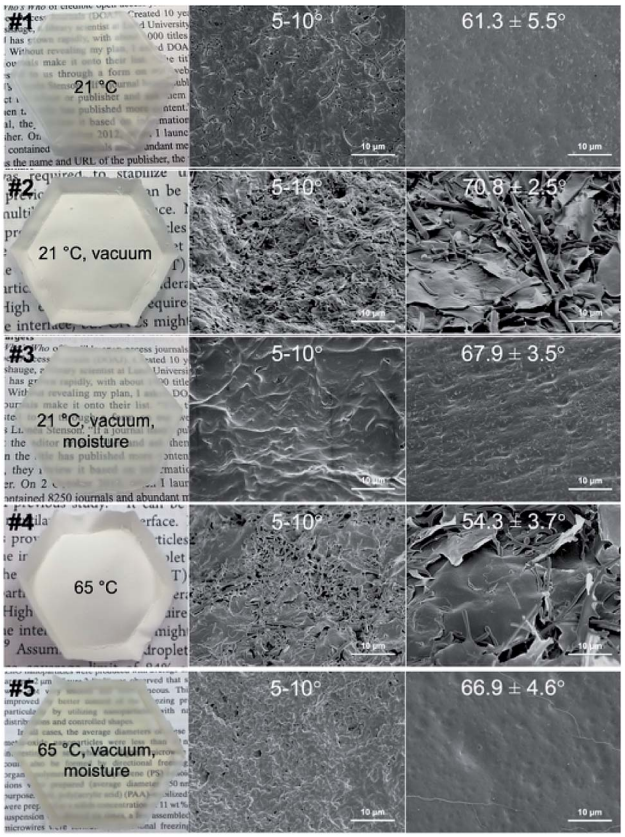

Fig. 1 Photographs (left) and SEM images of the top (middle) and bottom (right) surfaces of EtOH cast SPMF in PS weight boats and dried under varied conditions noted. Water contact angles ($N = 5$) on surfaces were denoted with SEM images.

porous, and thicker paper-like sheets (#2, #4), confirming much less association of SPMFs in the latter. The translucent appearance is indicative of absence of light-reflecting interfaces and close inter-microfibril association or fusion. The moisture effect was also consistent with the observations of rougher top air-exposed surfaces than the smoother bottom surfaces in contact with PS (Fig. S1, S3 and S5†) as opposed to the similarly rough top and bottom surfaces of those dry under low moisture level (Fig. S2 and S4†).

How SPMFs organize in relationship to the surfaces in contact was further elucidated by the water wetting contact angle measurements of top air-facing and bottom cast substrate-facing surfaces. All air-facing surfaces were similarly

Table 1 Ethanolic SPMF (1 w/v%, 10 mL) dispersions cast on hydrophobic PS under five conditions of temperature, relative humidity (RH), and vacuum: time taken to dry, appearance and thickness

Sample	Temp. (°C)	RH (%)	Vacuum	Time (h)	Appearance	Thickness (mm, $N = 3$)
1	21	30–35	No	72	Pale yellow, translucent	0.09 (±0.01)
2	21	30–35	Yes	16	Nearly white, opaque	0.17 (±0.02)
3	21	75–82	Yes	48	Pale yellow, translucent	0.06 (±0.02)
4	65	<8	No	2	Nearly white, opaque	0.17 (±0.03)
5	65	55–60	Yes	2	Pale yellow, translucent	0.06 (±0.02)

highly hydrophilic (WCA: 5°–10°), irrespective of their roughness or drying conditions. The bottom surfaces dried on the hydrophobic PS were remarkably more hydrophobic and slightly variable, ranging from 54.3° to 70.9° (Fig. 1). Water droplets wetted all the top surfaces immediately but retained the meniscus for *ca.* 2 min on the bottom surfaces of paper-like #2 and #4 (Fig. S6†). Water droplets placed on the bottom surfaces of the more hydrophobic films (#1, 3, 5) caused them to bend away and roll off. The more hydrophobic (66.9° and 67.9°) bottom surfaces of #3 and 5 films were relatively smooth with lower respective average RMS roughness of 44.0 nm and 37.6 nm than their rougher respective 138.8 nm and 164.0 nm RMS but hydrophilic (5°–10°) top surfaces (Fig. S7†). Therefore, the hydrophobic bottom surfaces of these films were attributed to their chemical nature, not topography.

SPMFs were also dried on a more hydrophilic glass Petri dish and an even more hydrophobic Teflon plate to further illustrate how the substrate surface hydrophilicity or hydrophobicity impacts the organization of SPMFs on which dried against. Faster drying under vacuum (#2) or with less moisture (#4) led both bottom glass-facing surfaces to be very hydrophilic (5°–10°), but their top air-facing surfaces had respective average WCA of 47.3 ± 4.1° and 26.3 ± 4.4° ($N = 5$). Intriguingly, SPMFs facing the highly hydrophilic and hydrogen bonding glass not only mimic the surface to be highly hydrophilic, but such organization also affected their top surfaces to be more hydrophobic than all those cast in the hydrophobic PS. Dried under condition of #1, the film bottom surface was so strongly adhered to the glass surface to be completely peeled off, a clear sign of the intense H-bondings formed during slow drying on the highly polar glass surface. The film dried on Teflon plate, on the other hand, showed similar water contact angles on the top air-facing surface (*ca.* 5°–10°) and bottom Teflon facing surfaces (*ca.* 50°–60°) as those on the PS under the same conditions. Interestingly, SPMFs organized similarly on the more hydrophobic Teflon as PS. As demonstrated, amphiphilic SPMFs have shown to reorient their hydrophobic and hydrophilic moieties according to the hydrophilicity or hydrophobicity of the substrates upon which to dry and as such the surfaces exposed to hydrophobic PS were moderately hydrophobic than the very hydrophilic top air-exposing surfaces. Drying on hydrophilic glass surface induce not only organization of hydrophilic SPMF moieties at the contact surfaces but affect across the entire 60 μm thickness to the air interface. More hydrophobic Teflon surface did not induce further hydrophobicity than PS.

The contact angle of a rough surface is defined by $\cos\theta^* = r\cos\theta$, where θ^* is the apparent contact angle at equilibrium state; θ is the Young's contact angle for the ideal surface of the same material; and r is the roughness ratio, which is the ratio of the true area to the apparent area of the surface or >1 for a rough surface. While surface roughness is known to reduce or increase the apparent wetting contact angle θ^* of respective hydrophilic or hydrophobic surfaces,[13] the small roughness differences between the relatively smooth top and bottom of the translucent films (#1, 3, 5) and those the highly porous paper-like top and bottom surfaces (#2, #4) had led to the conclusion that the different wetting behaviors between the top and bottom surfaces were attributed to their different surface chemical nature resulting from conformational orientation of amphiphilic SPMFs. Most intriguingly, highly hydrophilic surfaces (5°–10° WCA) to moderately hydrophobic surfaces (50°–70° WCA) can be produced from amphiphilic SPMFs by simply altering the hydrophilic (glass) or hydrophobic (PS, Teflon) nature of the casting surfaces.

Crystallinity, secondary structure composition and thermal behavior

The broad X-ray diffraction diagrams of all five 2D samples (Fig. 2a) were resolved into two major characteristic peaks at 2θ = 14.1–21.6° and 22.3–28.1° with respective 4.1–6.3 Å and 3.2–4.0 Å d-spacings assigned to the inner strand distance within α-helical and β structures and a minor one at 7.7°–9.0° (Table S1†) with equatorial reflection of 9.8°–11.5° correlated to the inter-sheet or inter-helix spacing.[14] All five were similarly crystalline with CrI of 50–56%, but significantly higher than FD SPs (41%). Similar FTIR amide I peak profiles (Fig. 2b) of all five indicated similar secondary structures with higher β-turns (#1, 2, 3) and β-sheets (#1, 3, 4, 5), consistent with their higher crystallinity (Fig. 2c). While slower drying at 21 °C showed consistently higher α-helical structure (#1, 2, 3), faster drying at 65 °C led to consistently higher β-sheets (#4, 5). To date, secondary structural transition of proteins to β-sheets has been extensively reported on silk fibroin by methanol[15,16] or EtOH[17] immersions and water vapor[18,19] or steam-autoclaving[20] annealing. Drying SPMFs in EtOH has shown to increase crystallization by 9–15%

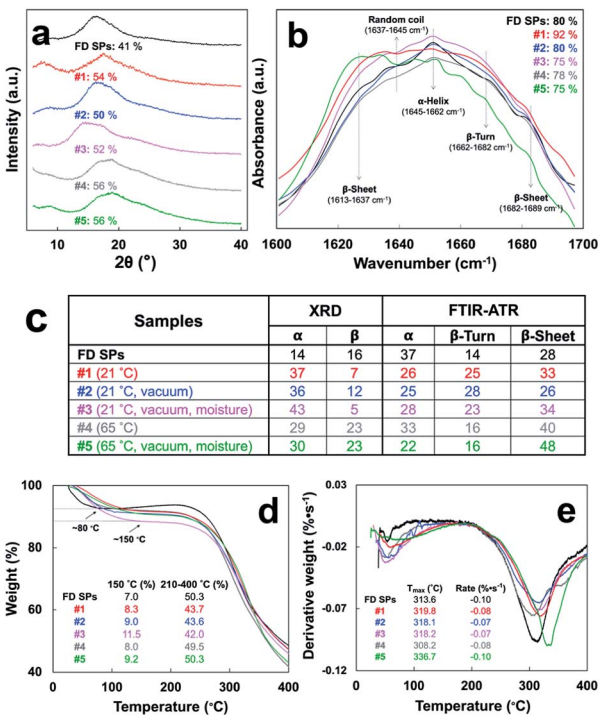

Samples	XRD		FTIR-ATR		
	α	β	α	β-Turn	β-Sheet
FD SPs	14	16	37	14	28
#1 (21 °C)	37	7	26	25	33
#2 (21 °C, vacuum)	36	12	25	28	26
#3 (21 °C, vacuum, moisture)	43	5	28	23	34
#4 (65 °C)	29	23	33	16	40
#5 (65 °C, vacuum, moisture)	30	23	22	16	48

FD SPs	150 °C (%)	210-400 °C (%)
#1	8.3	43.7
#2	9.0	43.6
#3	11.5	42.0
#4	8.0	49.5
#5	9.2	50.3

FD SPs	T_{max} (°C)	Rate (%·s⁻¹)
#1	319.8	-0.08
#2	318.1	-0.07
#3	318.2	-0.07
#4	308.2	-0.08
#5	336.7	-0.10

Fig. 2 Characteristics of EtOH cast SPMF: (a) XRD patterns with CrI values, (b) amide I peak by FTIR-ATR, (c) % secondary structure composition, (d) TGA, and (e) DTA.

in all cases, and annealing at 65 °C in the presence of moisture (#5), in particular, has shown to induce the highest secondary β-sheet structural transitions (48%) along with the highest crystallinity (56% CrI) for the first time, to the best of our knowledge.

All EtOH cast SPMF samples remained hygroscopic but contained slightly more bound water moisture, losing 8.0–11.5% more gradually at 150 °C as compared to 7.0% loss from FD SPs at 80 °C (Fig. 2d). All samples also decomposed at similar on set temperature *ca.* 215 °C but exhibited 4.5–6.2 °C higher peak degradation temperature (T_{max}) than FD SPs except for those dried at 65 °C (Fig. 2e). Particularly, the highest T_{max} of #5 may be attributed to its highest β forms.

Moisture regain and pH-responsive swelling behavior in aq. media

The hygroscopic EtOH cast SPMF samples absorbed increasing moisture with increasing RH, *i.e.*, 8.7 to 13.6%, 11.2 to 19.1%, and 53.4 to 68.2% at 30–35%, 65%, and 85–90% RH, respectively (Fig. 3a). While the translucent #1, 3 and 5 absorbed slightly more moisture at lower RH, the opaque paper-like #2 and 4 absorbed nearly 10% more moisture at 85–90% RH (Fig. 3a and Table S2†). While the moisture regain values of wool keratin and silk fibroin fibers were 14.0–19.0% and 11.0% at 65% RH, respectively, and reach 30% at 100% RH,[21] the moisture absorbing capacities of EtOH cast SPMF samples are similar at 65% RH but nearly double those natural protein fibers at 85–90% RH. These superior moisture-absorbing behaviors suggest significant inter-microfibril free or void volumes in these EtOH cast SPMF materials, irrespective of their macroscopic film-or paper-like structures.

All five EtOH cast SPMF samples conditioned at 65% RH and 21 °C would break upon folding at 180° but became foldable when conditioned at and above 80% RH, indicating their flexural strength to be strongly improved with substantially absorbed moisture. The glass transition temperature (T_g) of the most crystalline and structurally ordered #5 became more discernable with increasing presence of moisture from 0 to 30–35 and 85–90% RH, *i.e.*, the first T_{g1} dramatically decreased from 193.1 °C to 44.3 and −11.8 °C while the second T_{g2} slightly dropped from 222 °C to 212 °C and 208 °C, respectively (Fig. 3b). These two T_g may correspond to β-conglycinin and glycinin.[22] The below ambient temperature T_{g1} (−11.8 °C) affirms the plasticizing effect of bound moisture to explain the foldable and rollable ability of #5 in a highly humid environment. Such moisture dependent T_g suppression has been observed on silk cast films but at lower extents.[23]

Upon water immersion, only #3 and #5 remained intact for at least two weeks where the others either spontaneously disintegrated (#2, 4) or broken into pieces after 24 h (#1). Both #3 and #5 swelled instantaneously and with increasing pH from 0 to 10 in the planar directions to reach equilibrium within 5 min, losing less than 5% mass over two weeks, but completely disintegrated at pH 12 within 10 min. For #3 and 5, the planar swelling (S_p) was lowest at pH 3 (1.17 and 1.52), near the isoelectric point of SPs (PI = 4.51), much higher at pH 10 (1.87 and 1.59) and the highest S_p of *ca.* 2.24 at pH 1 (Fig. 3c and Table S3†). At pH 10, planar S_p of #3 would increase further to 4.13 and 4.63 after one and two weeks, respectively (Fig. 3c and Table S3†). Both could be air-dried to their original sizes and re-swollen similarly and remained resilient in water for at least another two weeks (Fig. S9†). Swelling in thickness was below 0.01 mm, the limit of Vernier scale used.

The outstanding pH-dependent swelling of #3 and 5 clearly reflects the amphoteric nature SPMFs that can be deprotonated into anionic $-COO^-$ or protonated into cationic $-NH_3^+$ below or above their PI, generating repulsive forces under extremely acidic (pH = 0) and basic (pH = 10) conditions. The wet resiliency may also be attributed to not only the high content of ordered secondary structures (84.5 and 85.9%) and CrI (both 56.0%) but also the higher degree of inter-microfibril fusion induced by moisture annealing (#3) and high temperature (#5).

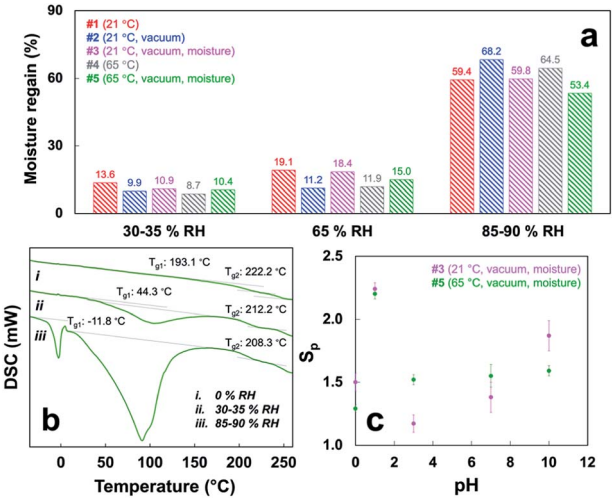

Fig. 3 Moisture and water effects on EtOH cast SPMF samples: (a) moisture regain values at different RH (detailed in Table S2†); (b) DSC of #5 conditioned at different RH; (c) planar swelling ratio (S_p, $N = 3$) of #3 and 5 at pH 0–10.

Controlled release of methylene blue (MB) *in vitro*

The controlled release of cationic MB bound to SP microfibrils cast in the same manner as #5 was studied. The frozen and freeze dried SP/MB (40 : 1, w/w) mixture was dispersed in EtOH as microfibrils in 1.2–1.3 μm widths and 20–100 μm lengths (Fig. 4a), similar to pristine SPMFs, and encapsulating *ca.* 94.1% MB.[10] The EtOH cast film of SP/MB microfibrils also exhibited swift pH dependent planar swelling (Fig. 4b), but slightly less (Tables S4 *vs.* S3†). MB releases at pH 1.5, 4.5 and 7.4 were monitored over time in three respective HCl/KCl, CH_3COOH/CH_3COONa, PBS buffers. At pH 7.4, MB was released at three stages of 7.53% in 5 min (stage I), then distinct 17.8% (stage II) and 31.9% (stage III) in 1.4 h and 168 h, respectively (Fig. 4c, d and Table 2). Overall, 57.2% MB was released and the substantially slower release in the III stage (31.9%, 168 h) is attributed to the deprotonation of carboxylic acid groups pH 7.4 (Fig. 4c, d and Table 2). Under

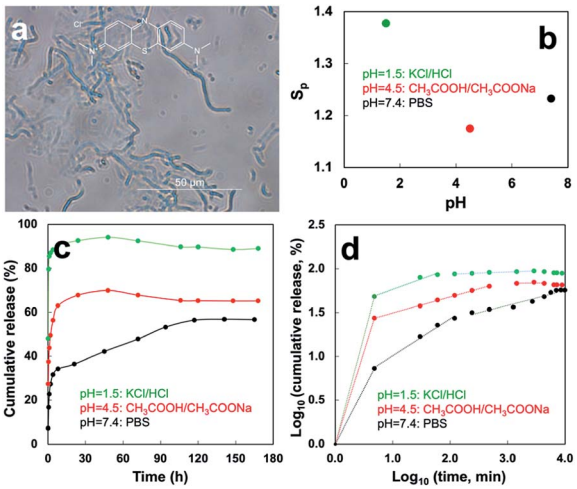

Fig. 4 (a) SPMFs with methylene blue (MB) encapsulated air-dried and imaged by the transmission microscopy (chemical structure of MB and image under the crossed polar inserted); SP/MB films (65 °C, vacuum, moisture) in PBS (pH = 7.4), CH_3COOH/CH_3COONa (pH = 4.5) and HCl/KCl (pH = 1.5) buffer *in vitro*: (b) planar swelling ratio (S_p); (c) cumulative release of MB; (d) Korsmeyer–Peppas model fitting of MB release.

extremely acidic pH 1.5, rapid release 48.8% MB occurred within the first 5 min, followed by another 36.4% in the next 1 h (Fig. 4c, d and Table 2), turning the originally dark blue SP/MB films to pale yellow (not shown). The highest 85.2% MB release in 1 h was attributed to protonation of the primary amines at pH 1.5 produces positive charges to not only repel cationic MB molecules but also cause the largest swelling (S_p = 1.38–1.49) (Table 2). At pH 4.5, 27.4% MB was released in 5 min then another 40.6% within 12 h (Fig. 4c, d and Table 2). A total 68.0% MB released in *ca.* 12 h was attributed to the weakly bound MB due to the almost zero net charge of SPs and slight swelling.

The cumulative release of MB at three pH levels fitted the Korsmeyer–Peppas model well with R^2 of 0.93–0.99 (Table 2 and Fig. S10†). The release exponent of MB was less than 0.5 except for the initial stage of burst release, corresponding to the quasi-Fickian diffusion mechanism that commonly observed in a polydisperse release system,[24,25] in which MB diffused through a swollen and positively/negatively charged matrix. This controlled release behavior of cationic MB may be extended to other cationic compounds as well as anionic species due to the amphoterism of SPMFs.

Experimental

Materials

Soy protein isolate (SPI, 92% protein) was purchased from MP Biomedicals, LLC. Hydrochloric acid (HCl, 1 N, certified), sodium hydroxide (NaOH, 1 N, certified), ethanol (EtOH, anhydrous, histological grade), sodium chloride (NaCl, certified), potassium chloride (KCl), acetic acid (CH_3COOH, certified), sodium acetate (CH_3COONa, certified) and methylene blue (MB) were all from Fisher Scientific. Sodium phosphate dibasic (99.95% trace metals basis) and potassium dihydrogen phosphate were purchased from Sigma-Aldrich. Regenerated cellulose dialysis membranes (3.5 kDa molecular weight cut-off, Fisherbrand, Pittsburgh, PA) were used for dialysis. All water used was purified by Milli-Q plus water purification system (Millipore Corporate, Billerica, MA). All chemicals were used as received without further purification.

Freeze-dried SP and SP/MB

Crude SPI was dispersed in water at 2 w% and dialyzed at 8–11 °C for 24 h. The dialyzed aqueous dispersion was diluted to 1 w% and blended at 30k rpm for 15 min using a high-speed blender (Vitamix 5200), cooled to ambient temperature, then centrifuged (5k rpm, 15 min) to collect the supernatant, so designated as colloids and stored at 8–11 °C. Aq. SP colloid at 1 w% or the mixture with MB (SP : MB = 40 : 1, w/w, 1.025 w%) were placed in 50 mL polypropylene centrifuge tubes to be frozen in liquid nitrogen (−196 °C, 5 min), then lyophilized (−50 °C, 2 days) in a freeze-drier (FreeZone 1.0 L Benchtop Freeze Dry System, Labconco, USA). The frozen and freeze-dried solids were referred as "freeze-dried or FD" for short from here on unless specified otherwise.

Preparation of film- or paper-like 2D structures

FD SPs were dispersed in ethanol (EtOH, 10 mL) at 1 w/v% by sonication (130 W, 5 min), then poured in hydrophobic polystyrene (PS) hexagonal weighing boat or Teflon dish, or hydrophilic Pyrex glass Petri dish, then dried at 21 °C (#1–3) or 65 °C (#4–5). Drying was accelerated by applying vacuum (#2, 3, 5) or slowed by the presence of water moisture (#3, 5) into the vacuum chamber whose relative humidity (RH) measured with

Table 2 Parameters of MB release *in vitro* fitted by Korsmeyer–Peppas model

pH	Release stage	Time (h)	Cumulative release (%)	Release exponent, n	Correlation coefficient, R^2
7.4	I	0.08	7.53	N.A.	N.A.
	II	1.4	17.8	0.42	0.9922
	III	167.7	31.9	0.17	0.9320
4.5	I	0.08	27.4	N.A.	N.A.
	II	11.6	40.6	0.18	0.9986
1.5	I	0.08	48.8	N.A.	N.A.
	II	0.7	36.4	0.24	0.9765

a digital humidity meter (Traceable Humidity Meter, Fisher Scientific, Hampton, NH, USA). Time taken to dry was recorded when automatic detachment from the substrate occurred. Cationic MB was bound to SP microfibrils by adding MB (0.025 w% or 0.08 mM) to 1 w% SP colloids to generate SP/MB (40 : 1, w/w) and the FD SP/MB were dispersed in EtOH and cast under same conditions as #5. All films were stored under 30–35% RH at 21 °C if unless otherwise specified. The thickness was read to the nearest 0.01 mm by a Vernier scale and their weight was measured using an analytical balance (Shimadzu, AUW220D) with an accuracy of 0.01 mg.

Characterization

Both sides of films/membranes were mounted with the conductive carbon tape and sputter coated with gold and observed using a field emission scanning electron microscope (FE-SEM) (XL 30-SFEG, FEI/Philips, USA). They were also stabilized on glass slides and scanned with the atomic force microscopy (AFM, MFP-3D, Oxford Instruments Asylum Research, Inc., Santa Barbara, CA) as reported in our prior work.[8] The root mean square (RMS) roughness was calculated based on scanning over a 5 μm × 5 μm area ($N = 5$) with 512 × 512 pixel resolution. Water contact angle ($N = 5$) of both surfaces of films was measured on different batches of samples using the drop shape analysis method to report the average and standard deviation.

X-ray diffraction (XRD) of FD SP and films/membranes was conducted on a Scintag XDS 2000 powder diffractometer using a Ni-filtered Cu Kα radiation (=1.5406 Å). The secondary structure composition of FD SP and films/membrane was evaluated by Fourier transform infrared attenuated total reflection (FTIR-ATR) on a Nicolet iN10 microscope spectrometer (Thermo Fisher Scientific, USA) using a liquid nitrogen cooled detector. Each spectrum was collected from 1700 to 1600 cm^{-1} at a 4 cm^{-1} resolution to characterize the amide I band that was deconvoluted to calculate the peak areas of specific secondary structure characteristic bands and the area percentage reported as the composition detailed in our prior work.[10] Thermal behavior of FD SP and films was evaluated using a differential scanning calorimeter (DSC-60, Shimadzu) and thermo gravimetric analyzer (TGA-50, Shimadzu) with Shimadzu thermal analysis system (TA-SOWSI). It was performed by heating at 10 °C min^{-1} under flowing N_2 at a 50 mL min^{-1} rate to 400 °C. Derivative thermogravimetric (DTG) curve was the first derivative derived from the TGA data.

The moisture regain of each film or membrane was determined by the percentage of mass gain following conditioning at 30–35%, 65%, and 85–90% RH at 21 °C for 24 h using an analytical balance (Shimadzu, AUW220D) with an accuracy of 0.01 mg over its dry weight at 0% RH and 150 °C. The swelling ratios of film strips (3 cm × 1 cm, *ca.* 30 mg) in water, aq. HCl (pH = 0, 1 or 3) or NaOH (pH = 10 or 12) at 21 °C as well as phosphate-buffered saline (PBS, pH = 7.4), CH_3COOH/CH_3COONa (pH = 4.5) or HCl/KCl (pH = 1.5) buffer at 37 °C were measured over a period of time. Upon removing from the aq. media at the prescribed time, each sample was gently wiped with Kimwipes to remove surface liquid and its width, length and thickness were measured by a Vernier scale to the nearest 0.01 mm and mass weighed. The planar (length × width), thickness and mass swelling ratios were calculated as the ratios of the corresponding values of swollen films to those of the original, and denoted as S_p, S_t and S_m, respectively. Three measurements were conducted to calculate the means and standard deviations.

FD SP/MB dispersions (0.1 w/v%, 10 μL) in EtOH were put on a glass slide and observed under a Leica DM2500 optical microscope equipped with the cross-polarizing filter. SP/MB films (*ca.* 20 mg) were respectively immersed in 25 mL phosphate-buffered saline (PBS, pH = 7.4), CH_3COOH/CH_3COONa (pH = 4.5) and HCl/KCl (pH = 1.5) buffer. The *in vitro* release of MB from SP/MB films (*ca.* 20 mg) was monitored by immersing in 25 mL phosphate-buffered saline (PBS, pH = 7.4), CH_3COOH/CH_3COONa (pH = 4.5) and HCl/KCl (pH = 1.5) buffer in a shaker bath at 37 °C. At predetermined time intervals, 1 mL solution was taken to quantify the amount of MB using Evolution 600 UV-vis spectrophotometer (Thermo Scientific) based on the calibration curve determined in the same aq. media. Then, 1 mL fresh buffer was added to the tubes to keep the volume consistently. The mechanisms of release from SP/MB films were investigated using a semi-empirical model known as the power law or the Korsmeyer–Peppas model[25] that is usually used to describe the drug release from a polymeric system,

$$\frac{M_t}{M_\infty} = kt^n$$

where M_t and M_∞ represent the amount of drug released at a time t at equilibrium, k is a constant characteristic of the release system, and n is the diffusion exponent characteristic of the release mechanism.

Conclusions

Thin 2D films and paper-like structures have been facilely cast from their ethanolic dispersions of amphiphilic and amphoteric SPMFs to exhibit tunable surface wettability and pH-responsive swelling behaviors. Most intriguingly, amphiphilic SPMFs organize at the cast substrate interface to generate corresponding hydrophilic or hydrophobic surfaces, mimicking that of the casting material. Surfaces cast on hydrophobic polystyrene were moderately hydrophobic with water contact angles (WCAs) of 54.3°–70.8° while those on hydrophilic glass and air-exposed surfaces are hydrophilic, showing 5°–10° WCAs. Water vapor annealing (55–60% RH) at moderately elevated temperature (65 °C) induce more ordered secondary structure from SPMF to produce film (#5) with 64% β structures, including 48% β-sheet form, and the highest CrI of 56%. Most significantly, this pristine SPMF film exhibited moisture-responsive T_g, pH-responsive planar swelling, and high wet resiliency under extremely acidic (pH 0) to highly basic (pH 10) conditions. Highly water-soluble cationic MB bound to SPMF films exhibited pH dependent release where a three-stage steady release at pH 7.4 followed a quasi-Fickian diffusion mechanism *in vitro*. This work shows the versatility of amphiphilic and

amphoteric SPMFs to be engineered into 2D structures with tunable surface hydrophilicity and hydrophobicity, moisture- and pH-responsive behaviors and controlled release capabilities that may be extended to other cationic and anionic species due to the amphoterism of SPMFs.

Conflicts of interest

There are no conflicts to declare.

Acknowledgements

The authors appreciate the support from USDA National Institute of Food and Agriculture, Hatch project CA-D-6706H and the Jastro Graduate Research Award from the University of California, Davis.

Notes and references

1 G. Kocak, C. Tuncer and V. Bütün, pH-Responsive polymers, *Polym. Chem.*, 2017, **8**(1), 144–176.
2 D. Schmaljohann, Thermo-and pH-responsive polymers in drug delivery, *Adv. Drug Delivery Rev.*, 2006, **58**(15), 1655–1670.
3 J. Shang, Z. Shao and X. Chen, Electrical Behavior of a Natural Polyelectrolyte Hydrogel: Chitosan/Carboxymethylcellulose Hydrogel, *Biomacromolecules*, 2008, **9**(4), 1208–1213.
4 J. Shang, Z. Shao and X. Chen, Chitosan-based electroactive hydrogel, *Polymer*, 2008, **49**(25), 5520–5525.
5 K. Tian, Z. Shao and X. Chen, Natural electroactive hydrogel from soy protein isolation, *Biomacromolecules*, 2010, **11**(12), 3638–3643.
6 Service FA, *Oil seeds: World market and trade*, U.S. Department of Agriculture, service, Fa, 2016.
7 M. Braun, I. Muñoz, J. H. Schmidt and M. Thrane, Sustainability of Soy Protein from Life Cycle Assessment, *FASEB J.*, 2016, **30**(suppl. 1), 894–895.
8 X. Liu and Y.-L. Hsieh, Amphiphilic and amphoteric aqueous soy protein colloids and their cohesion and adhesion to cellulose, *Ind. Crops Prod.*, 2020, **144**, 112041.
9 X. Liu and Y.-L. Hsieh, Amphoteric Soy Protein-Rich Fibers for Rapid and Selective Adsorption and Desorption of Ionic Dyes, *ACS Omega*, 2019, **5**, 634–642.
10 X. Liu and Y.-L. Hsieh, Amphiphilic protein microfibrils from ice-templated self-assembly and disassembly for Pickering emulsions, *ACS Appl. Bio Mater.*, 2020, **3**, 2473–2481.
11 A. Khdair, B. Gerard, H. Handa, G. Mao, M. P. Shekhar and J. Panyam, Surfactant– polymer nanoparticles enhance the effectiveness of anticancer photodynamic therapy, *Mol. Pharmaceutics*, 2008, **5**(5), 795–807.
12 M. Arias, E. López, A. Núñez, D. Rubinos, B. Soto and M. Barral, *et al.*, Adsorption of methylene blue by red mud, an oxide-rich byproduct of bauxite refining, *Effect of mineral-organic-microorganism interactions on soil and freshwater environments*, Springer, 1999, pp. 361–365.
13 R. N. Wenzel, Resistance of solid surfaces to wetting by water, *Ind. Eng. Chem.*, 1936, **28**(8), 988–994.
14 R. D. Rama and B. V. Gupta, Crystallite orientation in wool fibers, *J. Appl. Polym. Sci.*, 1992, **46**(6), 1109–1112.
15 I. C. Um, H. Kweon, Y. H. Park and S. Hudson, Structural characteristics and properties of the regenerated silk fibroin prepared from formic acid, *Int. J. Biol. Macromol.*, 2001, **29**(2), 91–97.
16 X. Hu, D. Kaplan and P. Cebe, Determining Beta-Sheet Crystallinity in Fibrous Proteins by Thermal Analysis and Infrared Spectroscopy, *Macromolecules*, 2006, **39**(18), 6161–6170.
17 Q. Lu, X. Hu, X. Wang, J. A. Kluge, S. Lu, P. Cebe, *et al.*, Water-insoluble silk films with silk I structure, *Acta Biomater.*, 2010, **6**(4), 1380–1387.
18 H. J. Jin, J. Park, V. Karageorgiou, U. J. Kim, R. Valluzzi, P. Cebe, *et al.*, Water-Stable Silk Films with Reduced β-Sheet Content, *Adv. Funct. Mater.*, 2005, **15**(8), 1241–1247.
19 X. Hu, K. Shmelev, L. Sun, E.-S. Gil, S.-H. Park, P. Cebe, *et al.*, Regulation of Silk Material Structure by Temperature-Controlled Water Vapor Annealing, *Biomacromolecules*, 2011, **12**(5), 1686–1696.
20 B. D. Lawrence, F. Omenetto, K. Chui and D. L. Kaplan, Processing methods to control silk fibroin film biomaterial features, *J. Mater. Sci.*, 2008, **43**(21), 6967.
21 International A. Standard Table of Commercial Moisture Regains for Textile Fibers, D1909-042004.
22 P. Chen and L. Zhang, New evidences of glass transitions and microstructures of soy protein plasticized with glycerol, *Macromol. Biosci.*, 2005, **5**(3), 237–245.
23 N. Agarwal, D. Hoagland and R. Farris, Effect of moisture absorption on the thermal properties of Bombyx mori silk fibroin films, *J. Appl. Polym. Sci.*, 1997, **63**(3), 401–410.
24 J. Siepmann and N. A. Peppas, Modeling of drug release from delivery systems based on hydroxypropyl methylcellulose (HPMC), *Adv. Drug Delivery Rev.*, 2001, **48**(2), 139–157.
25 R. W. Korsmeyer, R. Gurny, E. Doelker, P. Buri and N. A. Peppas, Mechanisms of solute release from porous hydrophilic polymers, *Int. J. Pharm.*, 1983, **15**(1), 25–35.